ARTICLES

Collisions of HCl with Rare Gas and Molecular Colliders

Elisabeth A. Wade,*,† K. Thomas Lorenz,‡ James L. Springfield,§ and David W. Chandler*

Combustion Research Facility, Sandia National Laboratories, Livermore, California 94551

Received: December 2, 2002; In Final Form: April 21, 2003

Collisions of HCl ($j = 0$) with rare gas and molecular colliders were studied using velocity-mapped ion imaging. For the rare gas colliders, Ne and Kr, the observed scattering behavior is very similar to that previously observed for HCl + Ar, and any differences are primarily due to the rule of corresponding states. For the molecular colliders, N_2 and CH_4, very different scattering behavior was observed, especially for high Δj_{HCl} transitions. When HCl is scattered into $j_{HCl} = 2$ or 3, the collision results in more forward-scattering than is observed for rare gas colliders, whereas when HCl is scattered into $j_{HCl} = 4$ or 5, the collision results in more backscattering. This implies that to generate HCl in a highly rotationally excited quantum state following collision with a diatomic or polyatomic collider, the collision must have a smaller impact parameter than would be required for an atomic collision.

I. Introduction

The use of spectroscopic techniques to study crossed molecular beam scattering has been both fruitful and difficult to accomplish. The advantage of using laser spectroscopy to detect crossed molecular beam scattering experiments is that one can obtain quantum-state-selective information about the scattering process. The disadvantage is that it is difficult to design an experiment with sufficient wavelength and spatial resolution and detection sensitivity. For this reason laser induced fluorescence (LIF) has been the dominant laser-based technique used for the detection of quantum-state-selective detection of scattering products.[1−5] Recently, the technique of ion imaging has been used to increase the sensitivity of spatially resolved ionization detection such that resonance enhanced multiphoton ionization (REMPI) can now be used to detect molecular beam scattering products.

In the 1990s, ion-imaging techniques were applied to reactive scattering in a single molecular beam by Buntine et al. [6] and to inelastic scattering in a bimolecular crossed-beam system by Suits et al.[7] Since then, ion imaging has been found to be a powerful tool for the study of bimolecular inelastic scattering. Ion imaging has been used to measure differential cross sections (DCS's),[7−10] as well as collision-induced rotational alignment[9] and orientation.[11] It has also been applied to several reactive systems, using both crossed molecular beam[12,13] and single beam[14] systems. In this work, ion imaging is applied to the collisions of HCl with rare gases and molecular colliders, at collision energies of ∼540 cm^{-1}. This is comparable to collision energies used in previous studies for the HCl + Ar system.[8]

Ar−HCl has been of interest to many groups over the last three decades. Andzelm et al. calculated potential energy surfaces for HCl + Ar, Kr, and Xe.[16] They found that the anisotropy and intermolecular range of the potential increased with the size and polarizability of the rare gas partner, resulting in increased rotational transfer efficiency. For a given Δj, a heavier collider will cause the rotational rainbow of HCl to be observed at smaller collision angles. Hutson and Howard have used high-resolution microwave spectroscopy to determine potential energy surfaces (PES's) for Kr−HCl and Ne−HCl.[17] Hutson later used coupled-channel bound-state calculations to further optimize the potential for Ne−HCl.[18] Velegrakis and Loesch have measured the DCS's for HCl + Kr, but at a higher collision energy and a lower angular resolution than in this study[19] However, the 1992 H6(4,3,0) Hutson semiempirical potential[15] incorporated a large body of spectroscopic data alongside detailed quantum calculations to produce the highest quality HCl + Ar PES to date. We will make use of this PES to compare collision systems of HCl with the rare gases and two other molecular colliders.

In the ion imaging technique, each image corresponds to a projection of all the velocity components in a single HCl rotational product channel. The products are found on a sphere in velocity space that we refer to as the scattering sphere. The scattering sphere is described by the Newton diagram, which is based on conservation of energy and momentum. The three-dimensional scattering sphere is projected to a two-dimensional imaging plane on the detector at the end of a time-of-flight tube. When HCl collides with a rare gas at modest energies, the only product states produced are excited rotational states in the scattered HCl molecules, because the atomic collider does not have internal energy. Each image, therefore, is the projection of a single scattering sphere with its velocity constrained by conservation of energy and momentum. When HCl collides with a molecular species, a number of rotational states in the collider can be activated for each excited rotational state produced in

* Corresponding authors: Elisabeth A. Wade, ewade@mills.edu, and David W. Chandler, chandler@california.sandia.gov.

† Permanent address: Department of Chemistry & Physics, Mills College, Oakland, CA.

‡ Permanent address: Lawrence Livermore National Laboratory, Livermore, CA.

§ Permanent address: Griffith University, Brisbane, Australia.

10.1021/jp027601s CCC: $25.00
Published on Web 05/30/2003

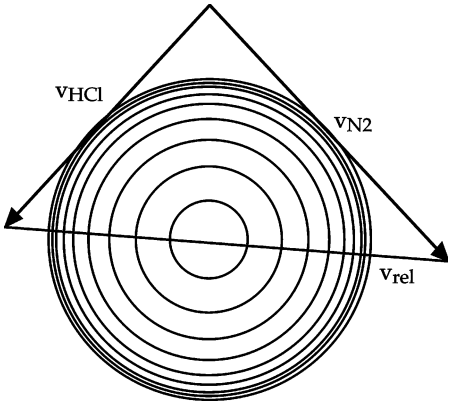

Figure 1. Schematic of overlapping Newton spheres. The outermost circle represents HCl ($j_{HCl} = 4$) correlated with N_2 ($j_{N_2} = 0$), and the inner circles represent HCl ($j_{HCl} = 4$) correlated with N_2 ($j_{N_2} = 2$, 4, 6−11). Initally, all j_{N_2} states are not shown because they are nearly coincident and would not be resolvable. The v_{rel} vector shows the "tilt" in the image resulting from the different velocities of HCl (seeded in Ar) and N_2.

the HCl scattered products. Each image is therefore the projection of multiple scattering spheres, each associated with a particular quantum state of the collider molecule. Figure 1 displays the Newton diagram for the HCl ($j = 0$) + N_2 → HCl ($j = 4$) + N_2 ($j = 0-11$) reaction showing the individual N_2 Newton spheres correlating to the particular quantum state of the HCl. Each observed product channel, indicated by an individual Newton sphere, can have a unique DCS and intensity pattern in the ion image. The rare gas collision systems give rise to scattering intensities on a single ring. The HCl + molecular colliders give rise to more complicated ion images that are a superposition of concentric scattering spheres. The concentric scattering spheres are centered about the center of mass for the particular scattering pair, with each ring corresponding to a pair of correlated product rotational states.

If the velocity spreads in the molecular beams were sufficiently narrow and initial collider rotational distributions sufficiently sharp, we would observe a series of concentric rings in the ion image corresponding to each set of correlated product states. The relative intensities of these rings provides information about the relative integral cross section as a function of Δj for the collider molecule. The intensity pattern within each ring gives information about the differential cross section for that pair of final rotational states. However, in these experiments the velocity spreads in the molecular beams are significant ($\Delta v/v \sim 10\%$ in each beam), the rotational states of the N_2 and CH_4 are closely spaced in energy, and the projection of the ion spheres onto the detector causes different channels to overlap. Therefore, in our data the concentric scattering rings associated with the rotational states of the N_2 or CH_4 overlap with their neighbors. This makes it difficult to extract the information about individual DCS's and correlated energy distributions cleanly and unambiguously. The larger the rotational constant of the collider, the greater the spacing between the Newton spheres, and the better the chance of extracting information from the overlapping rings. N_2 has a small rotational constant, 2.010 cm^{-1}.[20] CH_4 is a spherical top, with a rotational constant of 5.2412 cm^{-1}.[21] The collider masses are similar to those of Ne and Ar so that these collision systems are "kinematically equivalent" but have additional internal degrees of freedom.

II. Experimental Section

The experimental apparatus has been described previously.[8] In these experiments, HCl (seeded 2−5% in Ar) is the target gas. The rotational temperature of the HCl in the beam is low enough that about 97% of the HCl is initially in the $j_{HCl} = 0$ state and the remaining HCl is primarily in $j_{HCl} = 1$. Neat Ne (research grade, Spectra Gases), Kr (research grade, Matheson), N_2 (house nitrogen) and CH_4 (99.99%, Matheson) are used as collider gases. The collision energies depend on the collider gas, and these energies are summarized in Table 1. For the molecular collider studies, using pure gases in the collider beam resulted in a hotter molecular beam for the collider than for the target gas. A 2+2 REMPI spectrum was collected for N_2,[22] and the beam temperature was found to be 25 ± 5 K, which means that the rotational states up to $j_{N_2} = 3$ are substantially populated before the collision. The rotational temperature of the neat CH_4 molecular beam could not be directly measured as a REMPI scheme is not available. Although we have assumed it to be comparable to the N_2 rotational temperature, it is certainly possible that the beam temperature is substantially higher, as the rotational constant for methane is larger than that of N_2. Very pure CH_4 is necessary because the ionization laser caused the hydrocarbon impurities in the CH_4 molecular beam to nonresonantly dissociate and ionize, which results in a large background signal that is associated with the collider beam and cannot be easily subtracted.

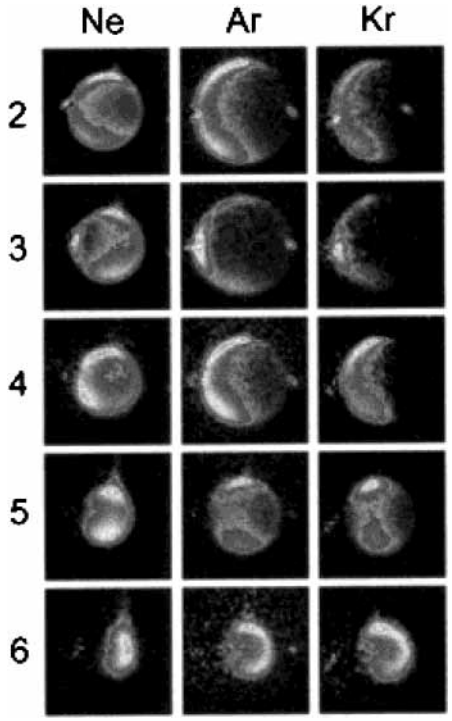

Figure 2. Ion images for HCl + Ne, Ar, and Kr. The images are rotated so that the relative velocity vector is horizontal.

TABLE 1: Collision Energy as a Function of Collider

collider gas	collision energy (±70 cm^{-1})
Ne	545
Kr	526
N_2	540
CH_4	549
Ar[8]	538

III. Results

IIIA. HCl + Rare Gas Images. The ion images for HCl collided with Ne, Ar, and Kr, with $\Delta j_{HCl} = 2-6$, are shown in Figure 2. The target beam, containing the HCl, is travelling to the left in the image whereas the collider beam is travelling to

the right. When HCl collides with Ar, the velocity of the target and collider beams in the laboratory frame are nearly identical. Therefore, the line of symmetry through the image, the relative velocity vector of the collision, appears horizontal in the ion images. When the collider gas is lighter than the carrier gas, as is Ne, the velocity of the collider beam is greater, and the line of symmetry is tilted so that the image appears to be rotated clockwise. Similarly, when the collider gas is heavier (Kr) than the carrier gas, the image appears to be rotated counterclockwise. The images in Figure 2 have all been corrected so that the relative velocity vectors are horizontal, to simplify comparisons between systems. $\Delta j = 1$ images are all extremely forward-scattered, and showed no collider dependence, and so will not be discussed here. Qualitatively, for a given Δj, the images are very similar. $\Delta j = 2$ is substantially side-scattered, with maximum intensity at $\Theta \sim 45°$. $\Delta j = 3$ is strongly forward-scattered. $\Delta j = 4$ is again side-scattered and is very similar to $\Delta j = 2$. $\Delta j = 5$ is purely side-scattered, with maximum intensity at $\Theta \sim 90°$. Finally, $\Delta j = 6$ is backscattered.

As described previously for HCl + Ar,[8] there are two background features in the HCl + Ne and HCl + Kr images. First, at 0°, there is a region of zero intensity. This occurs because, even though most of the HCl is initially in $j = 0$, some small amount is present in the molecular beam in excited rotational states even before the collision. Contributions to the scattering products from this rotationally excited HCl were subtracted from the ion image as the data were collected, as has been previously described.[8] For low Δj collisions, where the scattering sphere overlaps with the unscattered HCl, subtracting the unscattered HCl results in a "hole" in the scattering sphere. Second, in many images, a spot can be observed. For HCl + Ar, it is slightly outside of the scattering sphere; for HCl + Ne, it is further outside; and for HCl + Kr it is within the scattering sphere. This spot is due to the small amount of HCl remaining in the collider beam feed lines from a previous alignment step, and its position is indicative of the velocity of the collider beam.

IIIB. Comparison of Images of HCl + Molecular Colliders with HCl + Ar Images. The ion images for HCl + N_2 and HCl + CH_4 are shown in Figure 3, along with the previously published images of HCl + Ar. The target beam, containing the HCl, is travelling to the left in the image whereas the collider beam is travelling to the right. Because N_2 and CH_4 are both lighter than Ar their molecular beam velocities are greater and the image therefore appears rotated in the laboratory frame. Because the N_2 and CH_4 beams are moving on the images from left to right, this causes a clockwise rotation of the image. The images in Figure 3 have been rotated so that the relative velocity vector of the fragments is horizontal in the image. Some of these images appear to be slightly rotated because they are relatively noisy, and because the increased signal on the top half of the image relative to the bottom draws the eye upward, but these are artifacts.

The HCl + N_2 and HCl + CH_4 images are substantially different from the HCl + Ar images. First of all, the total signal (and therefore the integrated cross section) for these molecular colliders is much smaller than for HCl + Ar. The integrated cross-section, for a given j_{HCl}, is estimated to be 10−20 times smaller for HCl + N_2, and 100−500 times smaller for HCl + CH_4, on the basis of observed signals and required averaging time. The required averaging time varied, from ~30 min ($j_{HCl} = 2$ for HCl + N_2) to ~10 h ($j_{HCl} = 5$ for HCl + N_2). Also, ion images for the highest energetically accessible rotational states, $j_{HCl} = 6$ for HCl + N_2 and $j_{HCl} = 5$ and 6 for HCl + CH_4, could not be observed. We suspect that these rotational states were not observed because they were near the energetic limit of the collision, so that no rotatational energy would be available for the collider. This implies that high Δj_{HCl} is associated with high Δj for the collider.

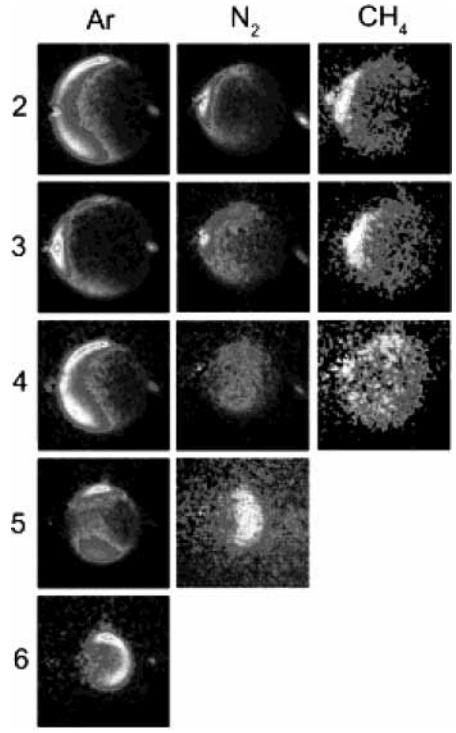

Figure 3. Ion images for HCl + Ar, N_2, and CH_4. The images are rotated so that the relative velocity vector is horizontal.

This implication is also supported by qualitative observations of the other images. For $j_{HCl} = 2$ and 3, the HCl + N_2 and HCl + CH_4 images have intense, narrow outer rings, very much like the HCl + Ar images, which suggests that relatively few rotational states of the collider are populated. For $j_{HCl} \geq 4$, on the other hand, the center of the HCl + N_2 and HCl + CH_4 images are much more filled in than the equivalent HCl + Ar images. This suggests that for high Δj_{HCl} many rotational states of the collider are populated, which further implies that the rotational energy is roughly equipartitioned between the collider and the target. This transition occurs fairly sharply, between $j_{HCl} = 4$ and 5 when N_2 is the collider and between $j_{HCl} = 3$ and 4 when CH_4 is the collider.

The HCl + N_2 images resemble the HCl + Ar images, but for higher Δj. In other words, the HCl ($j_{HCl} = 2$) + N_2 ion image resembles the HCl ($j_{HCl} = 3$) + Ar image, the HCl ($j_{HCl} = 3$) + N_2 image resembles the HCl ($j_{HCl} = 4$) + Ar image, etc. The HCl + CH_4 ion images are strongly forward-scattered for $j_{HCl} = 2$ and 3. This is why the HCl ($j_{HCl} = 2$, 3) + CH_4 images appear to have such poor signal-to-noise: at least 80% of the signal is concentrated in the first 20°.

IV. Discussion

IVA. Differential Cross Sections from Ion Images of HCl + Ne and HCl + Kr and Comparison of Theory. DCS's were extracted from each HCl + rare gas image, using an iterative method that has been described in detail previously and will be summarized here.[8] First, an isotropic DCS, $DCS(\theta) = 1$, is input into a scattering simulation program that produces a simulated image incorporating the apparatus function, including detectivity biases and the molecular beam spreads.

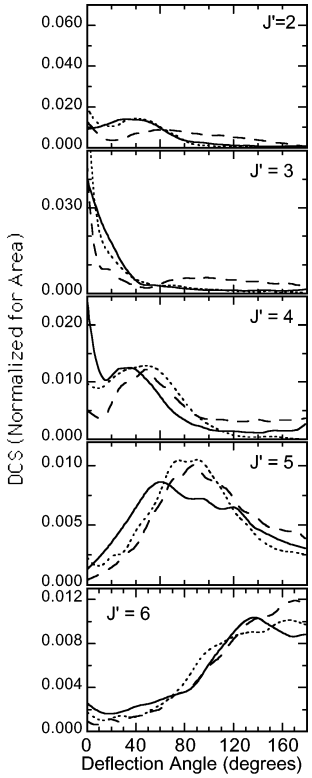

Figure 4. Extracted differential cross sections for HCl + Ne (dashed line), Ar (solid line), and Kr (dotted line).

Then, an annulus is defined around the rim of the experimental and simulated images and used to determine two angular intensity distributions. The experimental angular intensity distribution is divided by the simulated angular intensity distribution to produce the approximated DCS. The approximate DCS is then input back into the simulation to produce a new simulated image and a new angular intensity distribution, and the experimental angular intensity distribution is divided by the new simulated angular intensity distribution. This gives a correction function that is multiplied by the first approximated DCS to give a new DCS. This process continues until successive DCS's converge and the annulus around the rim of the simulated image matches to within experimental error the annulus around the experimental image. At this point, within our ability to model our experiment, we say the DCS has been determined.

DCS's for HCl + Ar (solid line), Ne (dashed line), and Kr (dotted line) are shown in Figure 4. Cursory inspection of the ion images seems to agree with the conclusion from an earlier study[19] that rare gases follow a simple kinematic scattering rule—HCl + Ne would produce more backscattering, whereas HCl + Ar and HCl + Kr would be increasingly forward-scattered. However, closer inspection of the DCS's shows that there is no simple progression. For $\Delta j = 2$ and $\Delta j = 3$, the HCl + Ne collision does show much more side-scattering and backscattering than HCl + Ar or HCl + Kr, and for $\Delta j = 3$, HCl + Kr is more forward-scattered than HCl−Ar. However, for $\Delta j = 4$, HCl + Ne and HCl + Kr are both slightly more backscattered than HCl + Ar. For $\Delta j = 5$ and $\Delta j = 6$, the images for the three systems appear to follow the expected progression, with HCl + Kr appearing more forward-scattered and HCl + Ne appearing more backscattered, but the extracted DCS's show nearly identical behavior. This apparent contradiction is in part an artifact due to the rotation of the Ne and Kr images. At the top center of each image, there is a bright spot, because in that region there is maximum overlap between the laser and the ions. The Kr images are rotated counterclockwise, so the spot appears to be forward-scattered, and the Ne images are rotated clockwise, so the spot appears to be backscattered. When the DCS's are extracted, we correct for the apparatus function and this effect disappears.

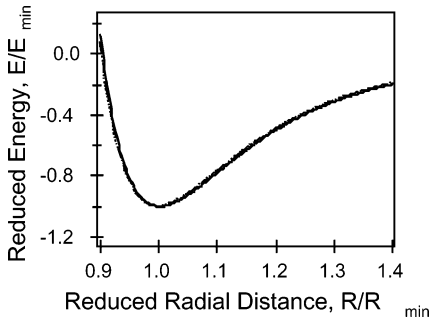

Figure 5. M5 quasi-isotropic potential energy surfaces for HCl + Ne (dashed line), Ar (solid line), Kr (dotted line), and Xe (dot−dashed line). Each surface is averaged over the angle between HCl and the rare gas atom and is then plotted in reduced coordinates. In reduced coordinates, these PES's are very nearly identical, and on this scale cannot be easily distinguished.

It is interesting to note that for $\Delta j = 2$, where the Hutson H6(4,3,0) potential predicted a sharp peak at 0°, whereas there is little forward-scattering observed for HCl + Ar, there is observable 0° scattering observed for HCl + Ne and HCl + Kr. It is possible that the forward peak for HCl ($\Delta j = 2$) + Ar is so narrow that it is completely obscured by the substantial amont of unscattered HCl subtracted out of the image.[8]

There is a good potential available for HCl + Ar, Hutson's H6(4,3,0) potential,[15] but similarly detailed potentials are not available for HCl + Ne or HCl + Kr. However, Hutson's older, M5 potential was available for Ne, Ar, Kr, and Xe,[18] so we began by comparing these potentials. Potential surfaces were modeled for these collision systems, on the basis of the analytical parameters of the M5 potentials, then used to generate a quasi-isotropic potential by averaging over the angle between the rare gas atom and HCl. The minimum of this quasi-isotropic potential was used to determine the radius and energy at that minimum point, and the values of R_{min} and E_{min} were then used to convert the potential surface into reduced coordinates, where R is replaced by R/R_{min} and E is replaced by E/E_{min}. These reduced PES's were compared in several ways: by qualitative comparisons of their contours, by comparison of the reduced quasi-isotropic potentials, and by comparisons of the PES's at specific angles, in particular 0, 90, and 180°. The four reduced quasi-isotropic potentials are shown in Figure 5. In Figure 5, as in all of our comparisons, the four PES's are nearly identical. Even for the hard wall ($R < R_{min}$), where the differences are largest, the reduced PES's agree within 10%. Though only the isotropic components are shown in Figure 5, the agreement for the angular dependence and the potential energy contours are also in excellent agreement for the reduced potential surfaces.

On the basis of the similarity of the reduced M5 PES's for all of the HCl + rare gas collision systems, we used a single PES to model all three collision systems. The H6(4,3,0) HCl−Ar program of Hutson[15] was used, without scaling, with the MOLSCAT program of Green and Hutson[23] to predict the DCS's for HCl + Ne, Ar, Kr, with the reduced mass adjusted for each system. In addition, adjustments were made for small changes in the center-of-mass collision energy unique to each experimental collision system. Collision energies of 550, 558, and 548 cm^{-1} were used for Ar, Ne, and Kr, respectively. The experimental collisional energy spread was handled by calculat-

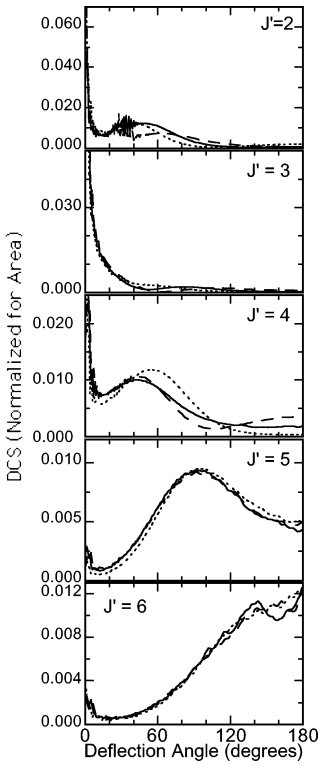

Figure 6. Theoretical differential cross sections for HCl + Ne (dashed line), Ar (solid line), and Kr (dotted line).

ing the DCS's at three collison energies: E_{cm} and ± 30 cm^{-1}, the experimental half-width half-maximum. The three calculations for each collision system were then weighted and averaged.

MOLSCAT's built-in angular expansion routine, the "VRTP mechanism", was implemented to generate the potential basis set of Legendre functions $P_\lambda(\cos\theta)$ up to and including $\lambda = 20$. The rotational basis set included all open channels and at least three closed channels for each collision energy seen in this study. All calculations used the full close-coupling method and HCl was treated as a linear rigid rotor. Integration of the coupling equations was handled by the hybrid log-derivative/Airy propagator of Alexander and Manalopoulos.[2] Integration limits were set to $R = 1.5$ Å at the inner turning point and carried out to at least $R = 25$ Å. Convergence was determined when successive steps in the total angular momentum contributed a negligible amount to the elastic and inelastic integral cross sections. Successive calculations using increasingly smaller cross-sectional convergence parameters were performed on the HCl−Ar system until no appreciable changes were observed in the DCS's. This convergence limit was 0.3 and 0.002 Å^2 for the elastic and inelastic cross-sections, respectively.

Although the comparison between the theoretical calculations and experimental observations is expected to be imperfect because we used a single unscaled potential for all three rare gas systems, it approximates the observed behavior exceedingly well. The predicted DCS's, with normalized area, are shown in Figure 6, with a solid line for HCl + Ar, a dashed line for HCl + Ne, and a dotted line for HCl + Kr. Although the agreement between theory and experiment is not perfect (which is not surprising because the agreement between the theory and experiment were not perfect for HCl + Ar[8]), it is remarkably impressive. The general features are very similar to the experimental DCS's shown in Figure 4. For $\Delta j = 2$, the theoretical calculation matches the predicted trend, with HCl + Kr showing a rotational rainbow slightly more forward-scattered (at ~35°) than that of HCl + Ar (at ~50°) or HCl + Ne (at ~70°). For $\Delta j = 3$, the three DCS's are very similar and primarily forward-scattered, but HCl + Ne does exhibit more scattering for $\Theta > 120°$ than HCl + Ar or HCl + Kr, as is observed experimentally. For $\Delta j = 4$, HCl + Ar and HCl + Ne are nearly identical, whereas HCl + Kr is actually slightly more backscattered, as observed. For $\Delta j = 5$, both experiment and the theoretical calculations show three DCS's with nearly identical rotational rainbows at ~90°. Finally, for $\Delta j = 6$, not only does the theory predict that all three DCS's are backscattered, but it predicts the peak and dip for HCl + Ar at ~130° while predicting the relatively smooth rise observed for both HCl + Kr and HCl + Ne. These results suggest that the potentials for HCl + Ne, Ar, and Kr are essentially the same, and that most of the differences between these systems are due to the rule of corresponding states, where the differences in the potential energy surface are primarily due to the differences in mass and relative velocity of the colliding system.

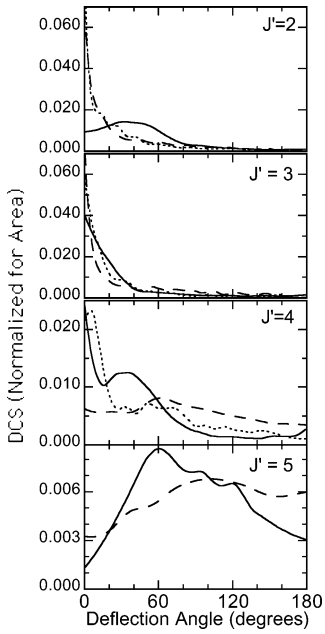

Figure 7. Extracted differential cross sections from the outer edges of the images of Figure 3. The outer edge correlates with low rotational state in the correlated scattered collider products. The solid line is HCl + Ar, the dashed line is HCl + N_2, and the dotted line is HCl + CH_4.

IVB. Differential Cross Sections from Ion Images of HCl + N_2 ($\Delta j < 5$) and HCl + CH_4 ($\Delta j < 4$). The DCS's for HCl + N_2 ($\Delta j < 5$) and HCl + CH_4 ($\Delta j < 4$) have been extracted, using the iterative procedure described previously and summarized above, and are compared with the DCS for HCl + Ar in Figure 7. The extracted DCS's displayed in Figure 7 are based on annuli set on the outer ring of the ion images, which corresponds to $\Delta j_{N_2} < 5$ and $\Delta j_{CH_4} < 4$. The solid line is HCl + Ar, the dashed line is HCl + N_2, and the dotted line is HCl + CH_4. Because each image consists of a superposition of several scattering spheres, each corresponding to a collider rotational state, it is very difficult to extract quantitative information from these images and we will restrict ourselves to a discussion of qualitative differences. The trends observed in the ion images can also be observed here. For low Δj_{HCl} ($j_{HCl} = 2$ and 3) the molecular colliders resulted in DCS's that are more forward-scattered than were observed for HCl + Ar, whereas for high Δj_{HCl} ($j_{HCl} = 4$ and 5) the molecular colliders resulted in DCS's that are more backscattered.

These differences are substantial and cannot be accounted for by the differences in kinematics or explained by the rule of corresponding states.[16] The implications of the HCl + CH_4

DCS's are particularly interesting, because the HCl is strongly forward-scattered when the methane has little internal energy (outer rim of image) even for $j_{HCl} = 4$. Although the internal states of CH_4 will complicate the analysis, the outer edge, where $\Delta j_{CH_4} < 4$, might be expected to show the same behavior as a monatomic collider, because CH_4 is a spherical top. Instead, the DCS's suggest that, even for relatively large Δj_{HCl} and low Δj_{CH_4}, HCl and CH_4 collisions are glancing, and do not result in large deflection angles. The HCl + N_2 DCS's are more difficult to interpret, but also suggest that the potential energy surface for HCl + N_2 is distinctly different from that of HCl + rare gases. Currently, our group is performing studies of NO + N_2 and NO + CH_4 collisions, and expect that these systems, in which the NO is probed via 1+1′ REMPI and which therefore produces images with substantially better signal-to-noise, will be amenable to more quantitative analysis.

V. Conclusions

We have observed and analyzed the correlated scattering patterns for collisions of HCl with three rare gas colliders, Ne, Ar, and Kr, a diatomic collider, N_2, and a polyatomic collider, CH_4.

For the atomic colliders, we find that the scattering behavior is very similar for all three rare gas colliders and that there is excellent agreement between the experimental DCS's and the theoretical DCS's predicted using the Hutson H6(3,4,0) potential for HCl−Ar,[15] scaled to account for mass and velocity differences between colliders. This strongly implies that the PES for the Ne−HCl, Ar−HCl, and Kr−HCl are extremely similar and that the only major differences are due to the rule of corresponding states.

For the molecular colliders, we find that, in general, the scattering is of lower intensity than the corresponding diatomic/atom collision. For HCl ($j_{HCl} = 2, 3$) being formed, we find that molecular colliders are more forward-scattered than atomic colliders. For HCl ($j_{HCl} = 4, 5$), however, we find the opposite trend. We find that for nitrogen as a collider, the scattering tends to be more backward-scattered than the corresponding diatomic/atom collision. When methane is the collider, the scattering not only is still more forward-scattered but also shows much more internal intensity due to rotational excitation in the collider molecule. This implies that to generate HCl in a highly rotationally excited quantum state with a diatomic or polyatomic collider, a smaller impact parameter is required compared to an atomic collision. Finally, we note that high Δj_{HCl} scattering products appear to be correlated with high Δj product states in the collider, whereas low Δj_{HCl} scattering products appear to be correlated with low Δj product states in the collider.

References and Notes

(1) Rettner, C. T.; Woste, L.; Zare, R. N. *Chem. Phys.* **1981**, *58*, 371.
(2) Hall, G.; Giese, C. F.; Gentry, W. R. *J. Chem. Phys.* **1985**, *83*, 5343.
(3) Krajnovich, D. J.; Butz, K. W.; Du, H.; Parmenter, C. S. *J. Chem. Phys.* **1989**, *91*, 7705.
(4) Keller, H. M.; Kulz, M.; Setzkorn, R.; He, G. Z.; Bergmann, K.; Rubahan, H. G. *J. Chem. Phys*. **1992**, *96*, 8817.
(5) Schreel, K.; ter Meulen, J. J. *J. Phys. Chem. A* **1997**, *101*, 7639.
(6) Buntine, M. A.; Baldwin, D. P.; Zare, R. N.; Chandler, D. W. *J. Chem. Phys.* **1991**, *94*, 4672.
(7) Suits, A. G.; Bontuyan, L. S.; Houston, P. L.; Whitaker, B. J. *J. Chem. Phys.* **1992**, *96*, 8618.
(8) Lorenz, K. T.; Westley, M. S.; Chandler, D. W. *Phys. Chem. Chem. Phys.* **2000,** *2*, 481.
(9) Cline, J. I.; Lorenz, K. T.; Wade, E. A.; Barr, J. W.; Chandler, D. W. *J. Chem. Phys.* **2001**, *115*, 6277.
(10) Kohguchi, H.; Suzuki, T. Alexander, M. *Science* **2001**, *294*, 832.
(11) Lorenz, K. T.; Chandler, D. W.; Barr, J. W.; Chen, W.; Barnes, G. L.; Cline, J. I. *Science* **2001**, *293*, 2062.
(12) Ahmed, M.; Peterka, D. S.; Suits, A. G. *Phys. Chem. Chem. Phys.* **2000**, *2*, 861.
(13) Liu, X.; Gross, R. L.; Suits, A. G. *J. Chem. Phys.* **2002**, *116*, 5341.
(14) Samartzis, P. C.; Smith, D. J.; Rakitzis, T. P.; Kitsopoulos, T. N. *Chem. Phys. Lett.* **2000**, *324*, 337.
(15) Hutson, J. M. *J. Phys. Chem.* **1992**, *96*, 4237.
(16) Andzelm, J.; Huzinaga, S.; Klobukowski, M.; and Radzio, E. *Chem. Phys.* **1985**, *1*, 100.
(17) Hutson, J. M. *J. Chem. Phys*., **1989**, *91*, 4448.
(18) Hutson, J. M.; Howard, B. J. *Mol. Phys.* **1982**, *45*, 769.
(19) Velegrakis, M.; Loesch, H. J. *Z. Phys. D* **1988**, *10*, 253−268.
(20) Herzberg, G. *Molecular Spectra and Molecular Structure, I. Spectra of Diatomic Molecules*; Van Nostrand Reinhold: New York, 1950; p 553.
(21) Herzberg, G. *Molecular Spectra and Molecular Structure, III. Electronic Spectra and Electronic Structure of Polyatomic Molecules*; Van Nostrand Reinhold: New York, 1966; p 619.
(22) Sitz, G. O.; Farrow, R. L. *J. Chem. Phys*. **1990**, *93*, 7883.
(23) Hutson, J. M.; Green, S. MOLSCAT computer code, version 14; Collaborative Computational Project No. 6 of the Engineering and Physical Sciences Research Council (U.K.), 1994.